Traveling Turing patterns in nonlinear neural fields

C. B. Price
Department of Physics, Katholieke Universiteit Leuven, Naamsestraat 61, B-3000 Leuven, Belgium
(Received 18 July 1995; revised manuscript received 6 February 1997)

Traveling pattern solutions to a nonlinear neural field are studied numerically and analytically. These occur in a homogeneous field without oscillatory or excitability properties, in a region of classical Turing instability. Our observations from one-dimensional and two-dimensional numerical experiments are reported and used to derive general existence conditions on both field structure and parameters, to support traveling patterns. These conditions are used to predict and observe novel traveling patterns catalyzed by the ''zero'' mode. A local bifurcation analysis is presented for traveling rolls in a field with pure-cubic nonlinearity. Our results are then placed in a broader context of nonlinear fields, and the biological significance is discussed.
[S1063-651X(97)10006-X]

PACS number(s): 64.60.−i, 47.20.Ky, 47.20.Lz, 87.10.+e

I. INTRODUCTION

Traveling waves and traveling wave fronts are well-known solutions to nonlinear spatially distributed systems, such as reaction-diffusion systems and neural nets. Wave-train solutions appear in systems with oscillating kinetics via Hopf bifurcation [1], and excitable media display solitary or trigger waves [2]. Even standing patterns in classical pattern-forming experiments have been observed to go traveling at a secondary bifurcation. Rayleigh-Bénard convection [3], directional solidification [4], the Faraday instability [5], and Couette flow experiments [6] have all shown this effect. A model for this drift bifurcation is presented in [7]. In this paper we report our observations of traveling pattern solutions in numerical experiments with scalar nonlinear neural fields where the nonlinearity is purely cubic. Traveling patterns appear spontaneously in a region of Turing instability from a variety of initial conditions. (The Turing instability usually refers to spontaneous symmetry breaking in reaction-diffusion systems to nonequilibrium structures with wavelength not directly linked to the field size. The great similarity between the description of reaction diffusion systems and our neural fields in the Fourier domain leads us to the more general application of the name Turing.)

We present a straightforward local bifurcation analysis of a one-dimensional (1D) pattern consisting of principal and third harmonic modes, and obtain constraints on the neural field structure and parameters to support these patterns. These parameter constraints are then generalized to 2D patterns consisting of an arbitrary number of modes. To illustrate the application of these constraints, we predict and discover a form of traveling pattern.

Consider a scalar neural field $u(\mathbf{x},t)\in\mathbb{R}$ defined in the plane $\mathbf{x}\in\mathbb{R}^2$ with the form

$$\frac{du(\mathbf{x},t)}{dt}=-\kappa u(\mathbf{x},t)+A\otimes f[u(\mathbf{x},t)]. \tag{1}$$

Here $u(\mathbf{x},t)$ is the average membrane potential at position $\mathbf{x}$ and time t. The nonlinear function $f(u)$ determines the neuron output, the pulse repetition rate. This is taken here as the polynomial $f(u)=\alpha u+\beta u^2-\gamma u^3$, and κ is the key (bifurcation) parameter. We shall take $\beta=0$ throughout this paper corresponding to a pure cubic (''pure-C'') field nonlinearity, and $\alpha=1$. While a sigmoid $f(u)$ is commonly used in neurophysiology, the above polynomial allows direct specification of nonlinear effects.

The operator $\otimes$ represents spatial convolution with kernel A, which determines the input connections to each neuron. Here these consist exclusively of recurrent feedback connections from nearby neuron outputs. We assume there is some form of lateral inhibition; nearby neurons are excitory and distant neurons are inhibitory in the feedback to each neuron input.

The spectrum F_k of the convolution kernel A then peaks around a principal spatial frequency k_p where it is positive in sign, and falls off for harmonics of this frequency. This is the classical recipe for production of patterns dominated by the principal spatial frequency, as κ moves the system through criticality. Various kernels A are used in our experiments, all with neurophysiological significance, such as the ''difference of Gaussian'' function (DOG) [8], the Gaussian derivative [9], or linear combinations of Gaussians.

Finally, the term $-\kappa u(\mathbf{x},t)$ represents the effects of the passive membrane input to each neuron. This field equation is well known in neural network literature, and was originally derived in the context of randomly connected neurons [10]. It is interesting that a random net is able to support traveling patterns; this is discussed in Sec. IV.

A typical example of a traveling pattern solution to Eq. (1) observed in our numerical experiments is seen in Fig. 1. The initial pattern comprised a small number of rolls of random phase and amplitude. It first developed into the canonical hexagonal structure, but shortly after approaching its expected stationary state of amplitudes, the hexagonal circle motif became egg shaped and the pattern proceeded to march vertically with uniform speed 9.3×10^{-2} rad/sec.

As the pattern moves at constant speed it maintains its asymmetric motif and the phases of the principal hexagonal pattern modes are seen to increase linearly with time; see Fig. 2.

Our analysis proceeds via the standard method of amplitude equation reduction [11,12]. With periodic boundary

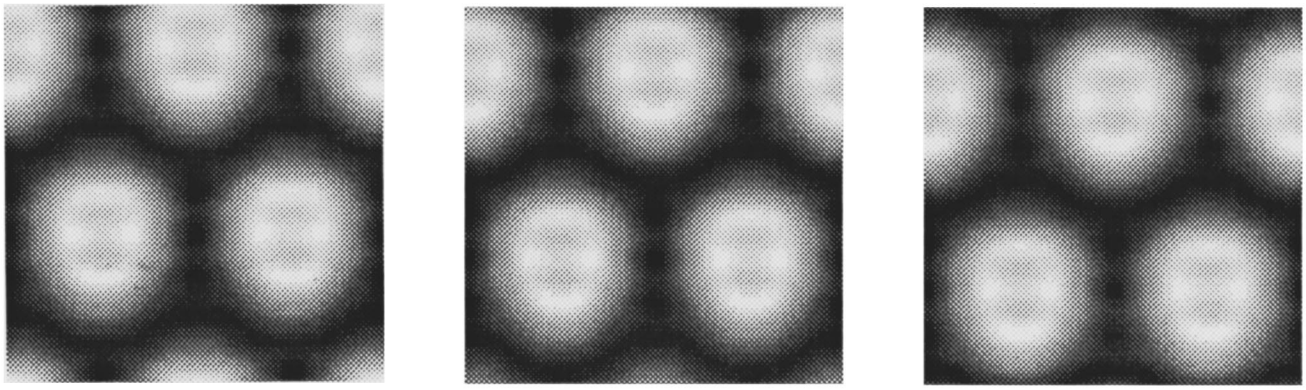

FIG. 1. Traveling hexagons in a 2D neural field shown with time increasing to the right. The canonical hexagonal resonant-triad pattern develops an egg-shaped motif and then travels downwards with speed 9.3×10^{-2} rad/sec. Parameters are given in the Appendix.

conditions, solutions to Eq. (1) are sought for as a sum of complex Fourier plane waves:

$$u(\mathbf{x},t)=\frac{1}{2}\,\xi_0(t)+\frac{1}{2}\sum_{j=1}^{\infty}\,[\xi_j(t)e^{i\mathbf{k}_j\cdot\mathbf{x}}+\xi_j^*(t)e^{-i\mathbf{k}_j\cdot\mathbf{x}}], \quad (2)$$

where the complex amplitude $\xi_j(t)$ of mode j and its conjugate $\xi_j^*(t)$ do not vary in space. They have wave vectors $\mathbf{k}_j$ and $-\mathbf{k}_j$, respectively. Mode $\xi_0\in\mathbb{R}$ is the ''zero'' or ''dc mode,'' representing a time-varying mean value of the field. The standard approach involving substitution of Eq. (2) into Eq. (1) yields a series of complex amplitude equations that can be further separated into real amplitudes A_j and phases ϕ_j using $\xi_j(t)=A_j(t)e^{i\phi_j(t)}$. Assuming the A_j have reached their stationary states, each component of Eq. (2) can then be written as $A_je^{i\mathbf{k}_j\cdot\mathbf{x}+i\phi_j(t)}$, and will satisfy a nondispersive wave equation if

$$\dot{\phi}_j(t)=\mathbf{c}\cdot\mathbf{k}_j, \quad (3)$$

where $\mathbf{c}$ is the wave velocity. Moreover, when all modes comprising a particular pattern satisfy Eq. (3) simultaneously, then the nonlinear pattern will advance coherently as a whole. Equation (3) leads to existence conditions, solution branches, and stabilities for traveling pattern solutions to amplitude equation representations of nonlinear fields. Figure 2 illustrates how the projection of the $\mathbf{k}_j$ onto $\mathbf{c}$ bring the $\dot{\phi}_j$ into relationship; the phase speeds of the principal hexagonal modes $\xi_{(2,1)}$ and $\xi_{(0,2)}$ are related by $\dot{\phi}_{(0,2)}=2\dot{\phi}_{(2,1)}$ for the observed vertical motion.

This paper is structured as follows. In Sec. II we begin by applying Eq. (3) to the simplest canonical pattern that may ''go traveling,'' the single roll. In a pure-C nonlinear field this can be most simply modeled by two Fourier modes, the *principal* mode ξ_p with wave vector $\mathbf{k}_p$ and the third harmonic ξ_{3p} with wave vector $\mathbf{k}_{3p}$. Using Eq. (3) we derive existence conditions, and also analyze the local bifurcation from the standing solution branch, producing results analogous to [13]. Comparisons with numerical experiments are made. The amplitude equation system is then extended to include ξ_{5p} with $\mathbf{k}_{5p}=5\mathbf{k}_p$ and a new existence condition obtained.

In Sec. III we generalize these results and derive an existence condition for patterns in 2D comprising an arbitrary number of modes. The section concludes by using the derived condition to predict the occurrence of a ''quadratic'' traveling pattern in the pure-C field.

In Sec. IV we place our results in a broader context of nonlinear fields, suggesting which type of field structure is necessary to support traveling waves. We also suggest how the field may model actual biological systems, in particular peristalsis in the digestive system. Details of all numerical experiments are found in the Appendix.

II. TRAVELING ROLLS IN A PURE-CUBIC FIELD

A. The ξ_p-ξ_{3p} system

Consider a field solution comprising the single roll ξ_p and its third harmonic ξ_{3p}. Assuming these are the only active modes, substitution of the sum (2) into Eq. (1) produces the amplitude equations

$$\dot{\xi}_p=\sigma_p\xi_p-\gamma F_p[\tfrac{3}{4}\xi_p|\xi_p|^2+\tfrac{3}{2}\xi_p|\xi_{3p}|^2+\tfrac{3}{4}\xi_p^*\xi_p^*\xi_{3p}], \quad (4)$$

$$\dot{\xi}_{3p}=\sigma_{3p}\xi_{3p}-\gamma F_{3p}[\tfrac{3}{4}\xi_{3p}|\xi_{3p}|^2+\tfrac{3}{2}\xi_{3p}|\xi_p|^2+\tfrac{1}{4}\xi_p\xi_p\xi_p].$$

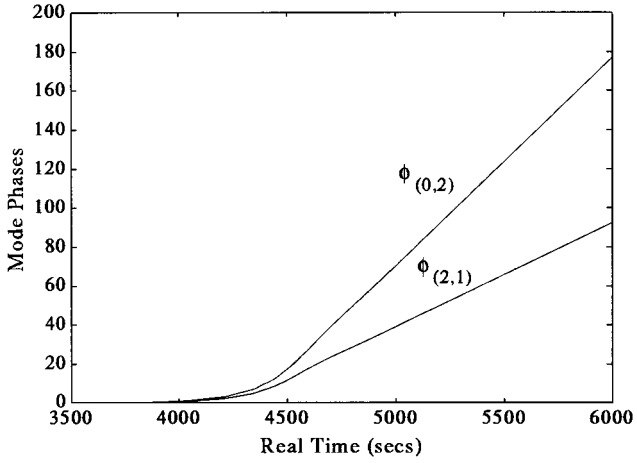

FIG. 2. Phase evolution for the principal components $\xi_{(0,2)}$ and $\xi_{(2,1)}$ of the vertically traveling hexagonal pattern in Fig. 1. Phase speeds $\dot{\phi}_{(0,2)}$ and $\dot{\phi}_{(2,1)}$ are in the ratio of their vertical components, 2/1. The onset of traveling occurs after the pattern has remained close to a stationary standing state for a long time, $\approx$4000 sec. See Fig. 5 for key to mode indices.

Here the $\sigma_j=(F_j-\kappa)$ are the linear growth rates, F_j the Fourier coefficient of convolution kernel A at frequency $\|\mathbf{k}_j\|$, and κ the bifurcation parameter. Terms $\frac{1}{4}\xi_p\xi_p\xi_p$ into ξ_{3p} and $\frac{3}{4}\xi_p^*\xi_p^*\xi_{3p}$ into ξ_p both arise from overlap of the four modes in the *interaction set* $\{\xi_p,\xi_p,\xi_p,\xi_{3p}^*\}$, whose wave vectors sum to zero, $3\mathbf{k}_p-\mathbf{k}_{3p}=0$. The mode equations (4) are best rewritten in terms of real amplitudes and phases for the principal A_p,ϕ_p and third harmonic A_{3p},ϕ_{3p} modes,

$$\begin{aligned}
\dot{A}_p&=\sigma_pA_p-\tfrac{3}{4}\gamma F_pA_p^2A_{3p}\cos(\phi_{3p}-3\phi_p)-\tfrac{3}{4}\gamma F_pA_p^3\\
&\quad-\tfrac{3}{2}\gamma F_pA_pA_{3p}^2,\\
\dot{\phi}_p&=-\tfrac{3}{4}\gamma F_pA_pA_{3p}\sin(\phi_{3p}-3\phi_p),\\
\dot{A}_{3p}&=\sigma_{3p}A_{3p}-\tfrac{1}{4}\gamma F_{3p}A_p^3\cos(\phi_{3p}-3\phi_p)-\tfrac{3}{4}\gamma F_{3p}A_{3p}^3\\
&\quad-\tfrac{3}{2}\gamma F_{3p}A_{3p}A_p^2,\\
\dot{\phi}_{3p}&=\frac{1}{4}\gamma F_{3p}\frac{A_p^3}{A_{3p}}\sin(\phi_{3p}-3\phi_p).
\end{aligned}\tag{5}$$

Looking for stationary solutions to Eq. (5), we recognize that amplitude and phase are differently flavored variables. Stationary solutions must have constant amplitudes $\dot{A}_j=0$, but their phases may be either constant ($\dot{\phi}_j=0$) or steadily increasing ($\dot{\phi}_j\neq0$). Solutions with $\dot{\phi}_p=\dot{\phi}_{3p}=0$ are standing patterns corresponding to $c=0$ in Eq. (3) and imply the fixed phase relation $\phi_{3p}-3\phi_p=n\pi$ between the modes. Solutions with $\dot{\phi}_p\neq0$, $\dot{\phi}_{3p}\neq0$, will form traveling patterns if they satisfy Eq. (3). Substitution of the phase equations into Eq. (3) shows this to be possible if

$$\frac{A_p^2}{F_p}+\frac{3^2A_{3p}^2}{F_{3p}}=0,\tag{6}$$

i.e., $F_pF_{3p}<0$. This is the condition for the existence of traveling patterns in the ξ_p-ξ_{3p} system. The system (5) has therefore the correct *structure* to support traveling patterns, and will do so if the parameters satisfy $F_pF_{3p}<0$. Condition (6) holds if $\sin\theta\neq0$: $\theta=\phi_{3p}-3\phi_p$; i.e., there exists a phase shift between the principal and harmonic modes. We interpret this phase shift θ as *driving* the individual phases ϕ_{3p},ϕ_p at differential rates to maintain pattern coherence. This phase difference is responsible for the slightly anisotropic appearance of the pattern motif (see Fig. 1), characteristic of our traveling waves. For the remainder of this paper we shall choose $F_p>0$, $F_{3p}<0$, and refer to modes with $F_j<0$ as ''*inverted*.''

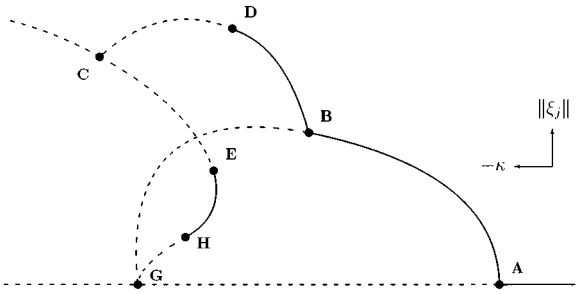

FIG. 3. Solution diagram for the ξ_p-ξ_{3p}-θ system where bifurcation parameter $-\kappa$ increases, from the primary bifurcation at A, to the left. The stable standing pattern branch AB is dominated by A_p close to A, and makes a secondary supercritical pitchfork bifurcation to traveling patterns BC. This branch loses stability at Hopf point D. A second standing branch bifurcates at G subcritically. This is dominated by A_{3p} near G, and turns around to briefly gain stability at Hopf point H.

It is straightforward to obtain an exact analytical solution for the traveling branch and its stability. To do this we use the dimension-3 system of two amplitudes A_p,A_{3p} and phase $\theta=\phi_{3p}-3\phi_p$ defined by

$$\begin{aligned}
\dot{A}_p&=\sigma_pA_p-\tfrac{3}{4}\gamma F_pA_p^2A_{3p}\cos\theta-\tfrac{3}{4}\gamma F_pA_p^3-\tfrac{3}{2}\gamma F_pA_pA_{3p}^2,\\
\dot{A}_{3p}&=\sigma_{3p}A_{3p}-\tfrac{1}{4}\gamma F_{3p}A_p^3\cos\theta-\tfrac{3}{4}\gamma F_{3p}A_{3p}^3-\tfrac{3}{2}\gamma F_{3p}A_{3p}A_p^2,\\
\dot{\theta}&=\frac{1}{4}\gamma\left(F_{3p}\frac{A_p^3}{A_{3p}}+9F_pA_pA_{3p}\right)\sin\theta.
\end{aligned}\tag{7}$$

These mode equations together with the condition (6) lead to the following closed-form solution for amplitudes of the traveling patterns:

$$A_p=\left(\frac{4}{3\gamma F_p}\right)^{1/2}\left(\frac{3F_p(1-3\mu^2)-4\kappa}{3(1-3\mu^4-4\mu^2)}\right)^{1/2},\tag{8}$$

where

$$\mu=\frac{A_{3p}}{A_p}=\frac{1}{3}\left(\frac{-F_{3p}}{F_p}\right)^{1/2},\tag{9}$$

and for the phase θ,

$$\cos\theta=\frac{(9\mu^4+20\mu^2+1)\kappa+9(\mu^4-\mu^2)F_p}{\mu[3F_p(1-3\mu^2)-4\kappa]}.\tag{10}$$

These results are comparable with those of Armbruster *et al.* [13] for the case of quadratic nonlinearity. We turn now to calculating the stability of these patterns. The Jacobian evaluated from Eq. (7) using Eq. (9) becomes

$$J_\theta=\frac{1}{4}\gamma F_pA_p^2\begin{bmatrix}-(6+3\mu\cos\theta) & -(12\mu+3\cos\theta) & 3\mu A_p\sin\theta\\ 9\mu^2(12\mu+3\cos\theta) & -9(\mu\cos\theta-6\mu^4) & -9\mu^2A_p\sin\theta\\ -18\mu\dfrac{\sin\theta}{A_p} & 18\dfrac{\sin\theta}{A_p} & 0\end{bmatrix}.\tag{11}$$

Requiring the real parts of the three eigenvalues to be negative generates the following constraints on parameter μ in the vicinity of the bifurcation point (with $F_{3p}<0$),

$$3\mu^4+4\mu^2-1<0,\quad\text{i.e.,}\quad\mu<\mu_1=0.464,\tag{12}$$

$$9\mu^4-2\mu-1<0, \quad \text{i.e.,} \quad \mu<\mu_2=0.722, \tag{13}$$

$$3\mu^4-18\mu^3-12\mu^2-2\mu-1<0, \quad \text{i.e.,} \quad \mu<6.62. \tag{14}$$

The first constraint subsumes the others and therefore determines the stability of the traveling pattern branch, and expresses this in terms of the ratio F_{3p}/F_p. The second and third constraints taken together make the upper left J_θ 2×2 ''block'' everywhere stable. It turns out that these two constraints also specify the stability of the *standing* pattern branch. To see this first note that J_θ is block diagonal at the bifurcation point ($\sin\theta=0$), with a 2×2 upper block and a zero lower 1×1 block. If the traveling branch is stable then this J_θ 2×2 block is also stable, by virtue of Eqs. (12) and (13). So at the bifurcation point there is a 1D nullspace associated with the lower block. But the standing branch has a block diagonal Jacobian along its entire length,

$$J_0=\frac{3}{4}\,\gamma F_p A_p^2\begin{bmatrix} -(2\pm\mu) & -(4\mu\pm1) & 0 \\ 9\nu^2(4\mu\pm1) & -3\nu^2(\pm1/\mu-6\mu^2) & 0 \\ 0 & 0 & \pm3\mu(1-\nu^2/\mu^2)\end{bmatrix}, \tag{15}$$

with $\mu=A_{3p}/A_p$, and $\nu=\frac{1}{3}(-F_{3p}/F_p)^{1/2}\neq\mu$ except at the bifurcation point where $\nu=\mu$. Here it inherits the stable J_θ 2×2 block and the 1D nullspace. Since J_0 is everywhere block diagonal it represents separate subsystems of amplitude (2×2 block) and phase, the latter associated with the lower 1×1 block, thus with the nullspace. We conclude that the standing pattern experiences a *phase* instability at the bifurcation point.

Conditions (12) and (13) completely specify the stability of branches straddling the local bifurcation. Note that the terms in Eq. (12) appear in the numerator of the expression for A_p, Eq. (8). This means that there is a supercritical pitchfork bifurcation to stable traveling branches if $\mu<\mu_1$, $\mu<\mu_2$ and a subcritical pitchfork to an unstable traveling branch if $\mu>\mu_1$, $\mu<\mu_2$. Both branches are unstable if $\mu>\mu_1$, $\mu>\mu_2$.

The local bifurcation is shown in the partial solution diagram Fig. 3. Standing pattern branch ABG emerges from the homogeneous state at A and bifurcates supercritically to the traveling branch BC. Initially stable, this branch loses stability at Hopf point D. Close to the bifurcation point A, branch AB solutions are dominated by large A_p. An unstable branch of standing patterns dominated by large A_{3p} bifurcates subcritically at G, turning around to recover stability at the Hopf point H. This joins to the traveling branch at C. The bifurcation points are calculated by substituting $\theta=0,\pi$ in Eq. (10):

$$\kappa_B=\frac{-9(\mu^4+\mu^3-\mu^2)+3\mu}{9\mu^4+20\mu^2+4\mu+1}\,F_p, \tag{16}$$

$$\kappa_C=-\frac{9(\mu^4-\mu^3-\mu^2)+3\mu}{9\mu^4+20\mu^2-4\mu+1}\,F_p. \tag{17}$$

Finally, the stability of the standing branch far from B can be calculated from the J_0 1×1 block. This is invariant to sign changes in $(A_pA_{3p}\cos\theta)$:$\theta=n\pi$, and so is Eq. (7). All branches AB:$\theta=n\pi$ therefore have the same stability. Also, this phase eigenvalue has a simple limit as the critical point is approached:

$$\lim_{\kappa\to F_p}\sigma_\theta=(F_{3p}-F_p), \tag{18}$$

requiring $F_{3p}<F_p$ to avoid a general phase instability. This is automatically satisfied here since $F_{3p}<0$.

B. 1D numerical experiments

Predictions of the above analysis were tested in numerical experiments solving the field (1) on the line discretized to 100 points (numerical details are given in the Appendix). Figure 4 shows a typical scenario of evolution from random initial conditions, first through a transient quasi-standing pattern, then to a stable traveling pattern. Amplitude and phase plots show clear initial competition between ξ_5 and ξ_6, won by ξ_5 when the third harmonic phase ϕ_{15} is driven into the traveling pattern condition. Thereafter the pattern runs with $\dot\phi_{15}/15\propto\dot\phi_5/5$. This is a stable pattern; nonresonant modes (e.g., ξ_6 and ξ_{10}) decay down to noise levels.

The stationary state field values are within around 10% of predicted values, e.g., for $\kappa=0.098$, $A_p(\text{field})=0.7175$, $A_p(\text{AE's})=0.763$ (where AE denotes amplitude equation), but bifurcation points differ significantly. These errors are traced to the large fifth harmonic ξ_{5p} component, and disappear when this is included in the amplitude equations; see Sec. II C.

The kernel used in these experiments was a weighted sum of three Gaussians (''tri-Gaussian'') and was computed in the frequency domain as

$$\text{TG}(k)=-w_1e^{-\sigma_1^2k^2/2}+(1+w_1)e^{-\sigma_2^2k^2/2}-e^{-\sigma_3^2k^2/2}, \tag{19}$$

with $\sigma_1=1.128$, $\sigma_2=2.82$, $\sigma_3=5.451$, $w_1=0.4$. This peaks at wave number $k=2\pi\times5/100$ ($F_p=0.339$) and has a significant inverted mode at $k=2\pi\times15/100$ ($F_{3p}=-0.186$). The reasons for building this kernel are detailed in Sec. IV; it is the simplest biologically meaningful kernel that has appreciable negative F_j.

C. Traveling rolls — the ξ_p-ξ_{3p}-ξ_{5p} system

The modes comprising the ξ_p-ξ_{3p}-ξ_{5p} representation form three resonant interacting sets, $I_1=\{\xi_p,\xi_p,\xi_p,\xi_{3p}^*\}$,

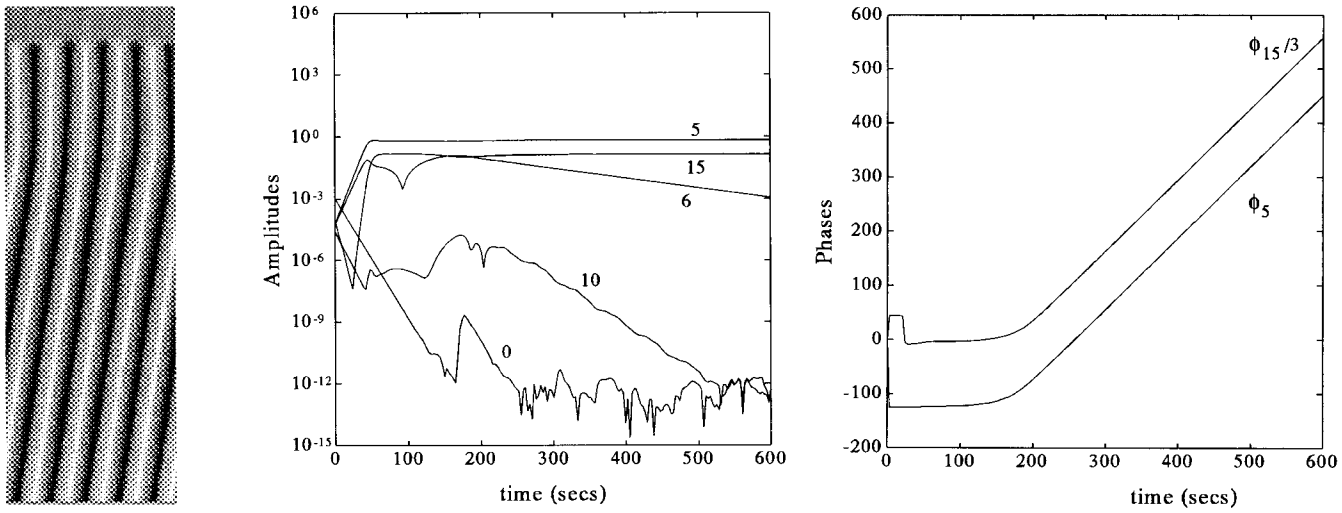

FIG. 4. Traveling solutions to the field (1) in 1D: Left: Space-time plot with time increasing vertically downwards shows evolution from random initial conditions ($\pm 10^{-4}$) through a transient state to the stable traveling state after $\approx$200 sec. Key amplitudes (center) and phases (right) show principal mode $A_p = A_5$ winning the competition over A_6 (and other modes) at the onset of traveling. The third harmonic A_{15} decays initially until its phase clicks into resonance with ϕ_5 whence A_{15} is driven by A_5 and rises. Nonresonant modes, e.g., A_{10} and A_0 decay to noise levels. Mode indices, used as labels, are wave numbers $\times 100/2\pi$.

$I_{\rm II}=\{\xi_p,\xi_p,\xi_{3p},\xi^*_{5p}\}$, $I_{\rm III}=\{\xi_p,\xi^*_{3p},\xi^*_{3p},\xi_{5p}\}$, which together with cross- and self-damping terms lead to the dimension-5 system

$$\dot\xi_p=\sigma_p\xi_p-\gamma F_p[\tfrac{3}{4}\xi^2_{3p}\xi^*_{5p}+\tfrac{3}{4}\xi_{3p}\xi^*_p\xi^*_p+\tfrac{3}{2}\xi_{5p}\xi^*_p\xi^*_{3p}+\tfrac{3}{4}\xi_p|\xi_p|^2+\tfrac{3}{2}\xi_p|\xi_{3p}|^2+\tfrac{3}{2}\xi_p|\xi_{5p}|^2], \tag{20}$$

$$\dot\xi_{3p}=\sigma_{3p}\xi_{3p}-\gamma F_{3p}[\tfrac{1}{4}\xi_p\xi_p\xi_p+\tfrac{3}{2}\xi_p\xi_{5p}\xi^*_{3p}+\tfrac{3}{4}\xi_{5p}\xi^*_p\xi^*_p+\tfrac{3}{2}\xi_{3p}|\xi_p|^2+\tfrac{3}{4}\xi_{3p}|\xi_{3p}|^2+\tfrac{3}{2}\xi_{3p}|\xi_{5p}|^2],$$

$$\dot\xi_{5p}=\sigma_{5p}\xi_{5p}-\gamma F_{5p}[\tfrac{3}{4}\xi^2_p\xi_{3p}+\tfrac{3}{4}\xi^2_{3p}\xi^*_p+\tfrac{3}{2}\xi_{5p}|\xi_p|^2+\tfrac{3}{2}\xi_{5p}|\xi_{3p}|^2+\tfrac{3}{4}\xi_{5p}|\xi_{5p}|^2].$$

This enhanced system has been studied numerically with the continuation software LOCBIF [14]. Solution branches around the standing-traveling bifurcation B retain their topology, but the positions of B and D are shifted. Agreement with field experiments is now better than 1%, e.g., for $\kappa=0.134422$, $A_p(\text{field})=0.650$, $A_p(\text{AE's})=0.649$, and $\dot\phi_5(\text{field})=2.29\times10^{-2}$, $\dot\phi_5(\text{AE's})=2.23\times10^{-2}$ rad/s, so Eq. (20) may be safely used to predict parameters for traveling patterns.

We now turn to the question of the existence of traveling solutions to this system, in particular we deduce conditions on the Fourier coefficients F_p, F_{3p}, F_{5p}. The strategy to be presented will be generalized in Sec. III to 2D patterns comprising M modes. First the phase equations for the $\dot\phi_j$ are extracted from the complex mode equations, multiplied by A_j^2, and written in matrix form using the 1D traveling wave condition $\dot\phi_j=ck_j$ to generate the right-hand side:

$$\begin{bmatrix} \frac{3}{4}A_p^3A_{3p} & \frac{3}{2}A_p^2A_{3p}A_{5p} & \frac{3}{4}A_{3p}^2A_{5p}A_p \\ -\frac{1}{4}A_p^3A_{3p} & \frac{3}{4}A_p^2A_{3p}A_{5p} & -\frac{3}{2}A_{3p}^2A_{5p}A_p \\ 0 & -\frac{3}{4}A_p^2A_{3p}A_{5p} & \frac{3}{4}A_{3p}^2A_{5p}A_p \end{bmatrix} \begin{bmatrix} \sin(\phi_{3p}-3\phi_p) \\ \sin(\phi_{5p}-\phi_{3p}-2\phi_p) \\ \sin(2\phi_{3p}-\phi_{5p}-\phi_p) \end{bmatrix} = c \begin{bmatrix} \dfrac{k_pA_p^2}{F_p} \\ \dfrac{k_{3p}A_{3p}^2}{F_{3p}} \\ \dfrac{k_{5p}A_{5p}^2}{F_{5p}} \end{bmatrix}. \tag{21}$$

Note that the qth column in this *phase matrix* contains terms generated by the qth interaction set I_q, and the jth row contains terms in the jth phase equation into $\dot\phi_j$. Clearly the phase matrix has rank equal to 2 reflecting the neutral stability of translation on the line: multiplying each row by its wave number k_j, writing $k_{np}=nk_p$ and adding produces the null row. Then the right-hand side sums to

$$\frac{k_pA_p^2}{F_p}+\frac{k_{3p}A_{3p}^2}{F_{3p}}+\frac{k_{5p}A_{5p}^2}{F_{5p}}=0. \tag{22}$$

This is the condition on the F_j's for the existence of traveling pattern solutions and extends the result (6) obtained above. It may be formulated as $F_pF_{3p}F_{5p}<0$ and requires the existence of an odd number of inverted modes. It is important to note that the addition of the fifth harmonic does not cause phase *locking* thus stopping the traveling; indeed it may induce it. Phase locking results when the rank deficiency of the phase matrix is removed by an additional interaction set that shares the same modes as an existing interaction set. Such sets are produced by *aliasing* in a spatially discretized system [15].

Asymmetric standing solutions to Eq. (20) have also been found using LOCBIF when $F_pF_{3p}F_{5p}>0$. Here the differences $\phi_{np}-n\phi_p\neq n\pi$ but $\dot{\phi}_{np}=0$, so that a standing but asymmetric pattern is produced. All such patterns found were unstable.

III. EXISTENCE OF TRAVELING ROLLS

A. General conditions on the F_j

The above result (22) can be extended to patterns consisting of an arbitrary number of modes in 1D or 2D. Consider N interaction sets involving a total of M modes, then M equations of the form $\Sigma_j\mathbf{k}_j=0$ can be written. But since (in 2D) all vectors can be expressed as a sum of two basis principal wave vectors $\mathbf{k}_p$ and $\mathbf{k}_q$, the system of M equations has rank $M-2$. There are therefore two degrees of freedom in phase variables that correspond to unconstrained positioning, or else direction of motion, of the pattern in the plane. Consider two general cubic interaction sets $I_B=\{\xi_j^*,\xi_k,\xi_l,\xi_m\}$ and $I_C=\{\xi_l^*,\xi_m,\xi_m,\xi_n\}$. Set I_B generates the following contributions to the phase equations:

$$\dot{\phi}_j=-a_{jB}F_j\frac{A_kA_lA_m}{A_j}\sin(\phi_j-\phi_k-\phi_l-\phi_m),$$

$$\dot{\phi}_k=a_{kB}F_k\frac{A_jA_lA_m}{A_k}\sin(\phi_j-\phi_k-\phi_l-\phi_m),$$

$$\vdots=\vdots. \tag{23}$$

Coefficients a_{jB} enumerate terms that are generated when the series (2) is substituted into the field (1), e.g., a contribution to a_{jB} is made when the selection integral

$$\xi_j^*\xi_k\xi_l\xi_m\int e^{-i(-\mathbf{k}_j+\mathbf{k}_k+\mathbf{k}_l+\mathbf{k}_m)\cdot\mathbf{x}}d\mathbf{x}\neq 0, \tag{24}$$

i.e., when $-\mathbf{k}_j+\mathbf{k}_k+\mathbf{k}_l+\mathbf{k}_m=0$. Multiplying the jth equation (23) by the associated A_j^2 transforms each term to a common amplitude factor $A_jA_kA_lA_m=\Pi A_B$ with common phase sum $\phi_j-\phi_k-\phi_l-\phi_m=\Sigma(\phi_B)$. Then Eq. (23) becomes

$$A_j^2\dot{\phi}_j=-a_{jB}F_j\prod A_B\sin\sum(\phi_B),$$

$$A_k^2\dot{\phi}_k=a_{kB}F_k\prod A_B\sin\sum(\phi_B), \tag{25}$$

$$\vdots=\vdots.$$

Using the condition on traveling waves $\dot{\phi}_j=\mathbf{c}\cdot\mathbf{k}_j$ on the left-hand side, the system of M phase equations can be written in concise matrix form, here with the addition of terms from the second interaction set I_C,

$$\begin{bmatrix} -a_{jB} & \\ a_{kB} & \\ a_{lB} & -a_{lC} \\ a_{mB} & a_{mC} \\ & a_{nC} \end{bmatrix}\begin{bmatrix}\prod A_B\sin\left(\sum\phi_B\right)\\ \prod A_C\sin\left(\sum\phi_C\right)\end{bmatrix}=\begin{bmatrix}\frac{\mathbf{c}\cdot\mathbf{k}_jA_j^2}{F_j}\\ \frac{\mathbf{c}\cdot\mathbf{k}_kA_k^2}{F_k}\\ \frac{\mathbf{c}\cdot\mathbf{k}_lA_l^2}{F_l}\\ \frac{\mathbf{c}\cdot\mathbf{k}_mA_m^2}{F_m}\\ \frac{\mathbf{c}\cdot\mathbf{k}_nA_n^2}{F_n}\end{bmatrix}. \tag{26}$$

Each column of the phase matrix contains terms generated by a single interaction set. Each row contains a phase equation into one mode. The coefficients a_{jQ} within each interaction set turn out to be proportional to the number of times mode ξ_j appears within that set. For example, in $I_C=\{\xi_l^*,\xi_m,\xi_m,\xi_n\}$ we have $a_{lC}=-1$, $a_{mC}=2$, and $a_{nC}=1$. These coefficients are in turn proportional to the coefficients of the wave vectors in the selection integral sum. For I_C this is $-\mathbf{k}_l+2\mathbf{k}_m+\mathbf{k}_n=0$. The result of all this is that since the wave vectors in each interaction set the sum to zero, multiplication of each row j in Eq. (26) by the corresponding wave vector $\mathbf{k}_j$ and summation over all rows will generate the null row. The right-hand side of Eq. (26) then also sums to zero to give

$$\sum_{j\in(B\cup C\cup\cdots)}\frac{\mathbf{k}_j(\mathbf{c}\cdot\mathbf{k}_j)A_j^2}{F_j}=0. \tag{27}$$

It is easy to show that when wave velocity $\mathbf{c}$ lies symmetrical with respect to the wave vectors, then this sum becomes

$$\sum_{j\in(B\cup C\cup\cdots)}\frac{(\mathbf{c}\cdot\mathbf{k}_j)^2A_j^2}{F_j}=0, \tag{28}$$

where the sign of each term is clearly the sign of the associated F_j. This is the general condition for the existence of traveling patterns in a 2D neural field with pure-**C** nonlinearity, and implies that there is at least one inverted mode $F_j<0$.

Application of Eq. (28) to the 2D pattern in Fig. 1 (with spectrum in Fig. 5), using the symmetry $F_{(-2,1)}=F_{(-2,-1)}$, etc., results in

$$\frac{A_{(-2,1)}^2}{F_{(-2,1)}}+2\frac{A_{(0,2)}^2}{F_{(0,2)}}+9\frac{A_{(-2,-3)}^2}{F_{(-2,-3)}}+4\frac{A_{(-4,-2)}^2}{F_{(-4,-2)}}+8\frac{A_{(0,4)}^2}{F_{(0,4)}}+81\frac{A_{(2,9)}^2}{F_{(2,9)}}=0, \tag{29}$$

which is satisfied since $F_{(2,9)}<0$.

The existence conditions (6), (22), and (28) partition mode *energy* (A_j^2) between modes. The total energy in the

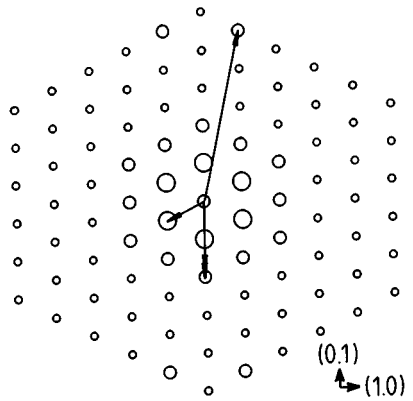

FIG. 5. Fourier spectrum of pattern in Fig. 1. Circle diameters indicate the relative sizes of the modes $\xi_{(u,v)}$ constituting the pattern. Zero frequency is in the center, surrounded by strong principal modes. Arrows show modes in the interaction set $\{\xi^*_{(2,9)},\xi_{(-2,-1)},\xi_{(0,-4)},\xi_{(0,-4)}\}$ which drive the traveling pattern. These clearly contain abnormally high energy.

normal modes equals that in the (few) inverted modes. A typical 2D pattern with a large spectral dimension will usually contain just a few inverted modes whose energy will then be relatively large. We can think of this energy as ''driving'' the traveling pattern. This is the case for Fig. 1 where the inverted modes $F_{(2,9)}<0$ and $F_{(-2,9)}<0$ contain abnormally large amounts of energy in their large A_j values, as clear from the spectrum Fig. 5.

B. $k-2k$ traveling patterns with pure-C nonlinearity

The above results will now be used to show the existence of $k-2k$ traveling patterns in a neural field lacking quadratic nonlinear terms, but with pure-C nonlinearity. The quadratic nonlinearity is usually invoked to support the $k-2k$ resonant interaction [7], but this is not in general necessary; we have previously shown that the dc or zero mode can actively couple to mediate an effective quadratic interaction in the case of standing patterns [16]. Here we shall show how this dc-mediated quadratic interaction can also support $k-2k$ traveling patterns. Interactions between the principal mode ξ_p, its harmonic ξ_{2p}, and the dc mode ξ_0 are described by the amplitude equations

$$\dot{\xi}_0=\sigma_0\xi_0-\gamma F_0[\tfrac{3}{4}\xi_p\xi_p\xi^*_{2p}+\tfrac{3}{4}\xi_{2p}\xi^*_p\xi^*_p+\tfrac{3}{2}\xi_0|\xi_p|^2+\tfrac{3}{2}\xi_0|\xi_{2p}|^2+\tfrac{1}{4}\xi_0^3],$$

$$\dot{\xi}_p=\sigma_p\xi_p-\gamma F_p[\tfrac{3}{2}\xi_{2p}\xi_0\xi^*_p+\tfrac{3}{4}\xi_p|\xi_p|^2+\tfrac{3}{2}\xi_p|\xi_{2p}|^2+\tfrac{3}{4}\xi_p\xi_0^2], \tag{30}$$

$$\dot{\xi}_{2p}=\sigma_{2p}\xi_{2p}-\gamma F_{2p}[\tfrac{3}{4}\xi_p\xi_p\xi_0+\tfrac{3}{2}\xi_{2p}|\xi_p|^2+\tfrac{3}{4}\xi_{2p}|\xi_{2p}|^2+\tfrac{3}{4}\xi_{2p}\xi_0^2],$$

which apart from self- and cross-damping terms contain the interaction set $\{\xi_0,\xi^*_{2p},\xi_p,\xi_p\}$ where ξ_0 is of course real. The wave vector sum $\mathbf{k}_0+2\mathbf{k}_p-\mathbf{k}_{2p}=2\mathbf{k}_p-\mathbf{k}_{2p}=0$ since $\mathbf{k}_0=0$. Applying Eq. (27) to this system gives

$$\frac{0^2A_0^2}{F_0}+\frac{1^2A_p^2}{F_p}+\frac{2^2A_{2p}^2}{F_{2p}}=0 \tag{31}$$

so that the dc mode drops out and $A_p^2F_{2p}=-4A_{2p}^2F_p$. The condition for the existence of traveling patterns is thus $F_pF_{2p}<0$ identical to that noted in [7] for the quadratic nonlinearity. Note from Eq. (31) that even though the dc mode is involved in the traveling pattern and contains energy, it does not share in the energy partitioning. This is consistent with its role as catalyst. Also, a sole inverted dc mode $F_0<0$ clearly cannot initiate traveling patterns.

IV. DISCUSSION

The conditions necessary for the existence of traveling patterns in a pure-C field have been deduced above in the spectral domain. Here we consider their implications for the field in physical space, in particular for the allowed field *structures*, which are able to support traveling patterns. The condition $\Pi_jF_j<0$ in the above analysis actually has two implications: firstly, that an inverted mode $F_j<0$ exists and, secondly, that the Fourier coefficients F_j *actually appear* as factors of each nonlinear term in the ξ_j amplitude equation; only then is the above analysis valid.

The first implication specifies the form of the connection kernel A. In engineering, negative Fourier coefficients are usually encountered as the result of truncation of the kernel extent in space. Since this may not have any biological relevance our kernels do not rely on spatial truncation. Instead, we constructed the simplest biologically meaningful kernel that generated significant inverted mode Fourier coefficients while not depending on spatial truncation. This was done using a weighted combination of three Gaussians, comprising a small central inhibitory region surrounded by a larger excitory region in turn surrounded by a larger inhibitory region Eq. (19). This can be thought of as a classical ''center surround'' kernel with an additional smaller inhibitory nucleus, or else as a concatenation of two difference of Gaussian kernels.

The second implication of our analysis, that the Fourier coefficients F_j actually appear as a factor in each nonlinear term in the ξ_j equations, translates directly into conditions on the *structure* of the field in physical space. For example, our analysis of the above field,

$$u_t=-\kappa u+A\otimes f(u), \tag{32}$$

generates amplitude equations of the form

$$\dot{\xi}_j=(\alpha F_j-\kappa)\xi_j+F_j[\beta\xi_k\xi_l-\gamma\xi_k\xi_l\xi_m], \tag{33}$$

where the F_j do appear in each nonlinear term, so that the field (32) can support traveling patterns. But our analysis applied to fields with structure

$$u_t=f(u)+A\otimes u \tag{34}$$

generates amplitude equations of the form

$$\dot{\xi}_j=(\alpha F_j-\kappa)\xi_j+\beta\xi_k\xi_l-\gamma\xi_k\xi_l\xi_m, \tag{35}$$

where the F_j do not appear in the nonlinear terms. This field will not support inverted-mode generated traveling patterns. Note that the Swift Hohenberg equation is of the latter type and so will not support traveling Turing patterns. The other important class of field that does have the correct structure is reaction-diffusion systems

$$\mathbf{u}_t = \mathbf{f}(\mathbf{u}) + \mathbf{D}\nabla^2\mathbf{u}, \tag{36}$$

which generate amplitude equations of the form

$$\dot{\xi}_j^{(a)} = \sigma_j^{(a)}(\kappa)\xi_j^{(a)} + Q_{jkl}^{(abc)}(\kappa)\xi_k^{(b)}\xi_l^{(c)} + C_{jklm}^{(abcd)}(\kappa)\xi_k^{(b)}\xi_l^{(c)}\xi_m^{(d)}, \tag{37}$$

where a,b,c,d select the vector field components [11]. Here the interaction coefficients $Q_{jkl}^{(abc)}$ and $C_{jklm}^{(abcd)}$ depend on the mode wave numbers, and may go negative, providing an equivalent condition to $\Pi_j F_j < 0$. We expect our traveling patterns to be found in reaction-diffusion systems.

An intriguing and important question naturally arises. Is there any biological significance of our results, in particular the existence of traveling patterns in a random homogeneous neural network? Periodic and traveling patterns such as insect gait, swimming fish, and feeding action in crustaceans have indeed been extensively studied, and associated neural circuitry discovered. But these neural circuits are formed out of dedicated ''central pattern generators,'' small groups of neurons that once initiated by a control signal from the central nervous system drive the motor neurons and attached muscles. The gastric system of decapod crustaceans [17] consists of some 30 neurons ''hardwired'' with specific interconnections. Different rhythmic activity is obtained according to levels of chemical neuromodulators. The swimming control of the lamprey [18] consists of repeated segments of hardwired neurons with specific connections. A distributed central pattern generator.

These examples contrast markedly with the random homogeneous connections of our neural field, which lacks totally specific, dedicated, hardwired connections. There is, however, one nervous system that does resemble our neural field. This is the enteric nervous system (ENS) which controls bowel movements. Although the neural circuitry is still being actively researched, it clearly consists of a network of motor, sensory, and interneurons embedded between the longitudinal and circular muscles of the bowel. This structure supports slow, almost sinusoidal, traveling electrical waves by reflex activity [19,20]. In a series of elegant papers, Miftakhov *et al.*, have modeled the electrophysiological, mechanical, and pharmacological aspects of the ENS [21,22]. They model the intestine as a series of repeated functional modules, with full specification of the mechanical and electrophysiological details: a distributed pattern generator.

Our field Eq. (1) provides a different sort of model for the ENS, at the level of a *generic* description. No electrophysiological details are specified; the model provides a ''shell'' that via its predictions may help guide the search for the anatomical and physiological details. The main prediction of our model is that the most likely neural circuitry contains a distribution of axon or dendrite projections with three characteristic scales. This circuitry could be provided by interstitial cells. These could generate traveling waves, which would drive the motor neurons of the intestine muscles. A secondary prediction concerns the *shape* of the observed waves, which, as a consequence of the phase-driving mechanism, must be slightly anisotropic, not exactly sinusoidal. The various operating modes, peristalsis (traveling waves), mixing (standing waves), and ileus (quiescent state) appear as branches in our solution diagram.

V. CONCLUSIONS

Observations of traveling Turing patterns in pure-C neural fields have been described and tools developed to allow their prediction. In particular, the existence conditions on field structure and parameters have been derived for a general case, these have been used to find novel dc-catalyzed $k-2k$ patterns. A local bifurcation analysis has been made for traveling rolls. These patterns bifurcate by a phase instability, which is manifested as a breakdown in the phase linking of ϕ_p to ϕ_{3p} by $\phi_{3p}-3\phi_3 = n\pi$ for standing patterns, the harmonic mode being repelled away in space. This mode then miraculously finds a stable configuration with the principal mode. The stability originates in interactions between amplitudes and phase, which in effect remove the block diagonal structure from the system Jacobian, lowering σ_θ below zero, and stabilizing the traveling pattern. In short, the onset of traveling patterns is due to a phase instability, their stable existence is ensured by nonlinear amplitude-phase interactions.

ACKNOWLEDGMENTS

We thank Professor A. Oosterlinck for interest in and support of this work, and G. Dewel and P. Borckmans of the Université Libre de Bruxelles for bringing additional material to our attention.

APPENDIX

Numeric experiments on the field (1) were performed by discretizing the field and integrating the system of ODE's obtained as a function of time. Adaptive Runge-Kutta and Stiff (backward differentiation formula) methods were employed in parallel to obtain checks. The convolutions for the 1D experiments were performed in the Fourier domain, after a standard fast Fourier transform. This removed any problems associated with aliasing of pattern components. The 2D experiments were made with direct convolution in the physical space domain. The fundamental pattern frequency was small enough to avoid generation of significant aliasing components.

Parameters for 2D traveling pattern (Fig. 1)

The difference of Gaussian convolution in 2D was calculated as the difference between the field convolved with the separate ''inner'' and ''outer'' Gaussian components. Each 2D Gaussian convolution was performed as the composite of two separated 1D Gaussian convolutions, in the x and y directions. This ''separable'' convolution technique is efficient. Each 1D convolution mask was calculated as

$$G(x)=\frac{1}{\sqrt{2\pi}\sigma}\,e^{-(x-x_c)^2/2\sigma^2}, \tag{A1}$$

where the inner and outer width parameters were $\sigma_i=12.5/\sqrt{2}$, $\sigma_o=12.5$. Each kernel was sampled at the points up to a distance $\pm 2\sigma$ relative to its center x_c. The 2D field $u(\mathbf{x},t)$ was discretized on 100×100 pixels^2. Field parameters were; $\alpha=1$, $\beta=0$, $\gamma=1.5$, $\kappa=0.018$.

Parameters for 1D traveling pattern (Fig. 4)

Here the kernel was defined as a ''tri-Gaussian.'' This is a weighted sum of three Gaussians, and is computed in the frequency domain as

$$\mathrm{TG}(k)=-w_1e^{-\sigma_1^2k^2/2}+(1+w_1)e^{-\sigma_2^2k^2/2}-e^{-\sigma_3^2k^2/2}, \tag{A2}$$

where here $\sigma_1=1.128$, $\sigma_2=2.82$, $\sigma_3=5.451$, $\omega_1=0.4$, and $\alpha=1.0$, $\beta=0.0$, $\gamma=1.5$, $\kappa=0.134422$. The kernel can also be conceived as a weighted difference between two difference of Gaussian kernels. The field was discretized to 100 points, the pattern had principal wave number $k_p=(2\pi)\times 5/100$.

3. Parameters for dc-mode catalyzed traveling pattern

A representative example can be computed using a weighted combination of a Gaussian function with its second and fourth derivatives (G-GD). In the frequency domain this is

$$\text{G-GD}(k)=10.0[k^2(1-k^2w_1)-w_2]e^{-\sigma^2k^2/2} \tag{A3}$$

with kernel parameters $\sigma=3.8$, $\omega_1=3.6$, $\omega_2=0.01$ and field parameters $\alpha=1.0$, $\beta=0.0$, $\gamma=1.5$, $\kappa=0.05406$. A traveling pattern with wave number $(2\pi)\times 5/100$ emerges in a field of discretization 100 pixels.

[1] K. Kuramoto, *Chemical Oscillations, Waves and Turbulence* (Springer-Verlag, Berlin, 1984).
[2] V. S. Zykov, *Modelling of Wave Processes in Excitable Media* (Manchester University Press, Manchester, 1988).
[3] R. W. Walden, P. Kolodner, A. Passner, and C. M. Surko, Phys. Rev. Lett. **55**, 496 (1985).
[4] A. J. Simon, J. Bechhoefer, and A. Libchaber, Phys. Rev. Lett. **61**, 2574 (1988).
[5] S. Duady, S. Fauve, and O. Thual, Europhys. Lett. **10**, 309 (1989).
[6] I. Mutabazi, J. J. Hegseth, C. D. Andereck, and J. E. Wesfreid, Phys. Rev. A **38**, 4752 (1988).
[7] S. Fauve, S. Duady, and O. Thual, J. Phys. (France) II **1**, 311 (1991).
[8] C. Enroth-Cugell and J. G. Robson, J. Physiol. **187**, 517 (1966).
[9] R. A. Young, Spatial Vision **2**, 273 (1987).
[10] S. Amari, Biol. Cybernetics **27**, 77 (1977).
[11] H. Haken, *Advanced Synergetics* (Springer-Verlag, Berlin, 1993).
[12] P. Manneville, *Dissipative Structures and Weak Turbulence* (Academic Press, New York, 1990).
[13] D. Armbruster, J. Guckenheimer, and P. Holmes, Physica D **29**, 257 (1988).
[14] A. I. Khibnik, Y. A. Kuznetsov, V. V. Levitin, and E. V. Nikolaev, Physica D **62**, 360 (1993).
[15] C. B. Price, Ph.D. thesis, K. U. Leuven (unpublished).
[16] C. B. Price, Phys. Lett. A **194**, 385 (1994).
[17] P. S. Katz and R. M. Harris-Warrick, Trends Neurosci. **13**, 367 (1990).
[18] S. Grillner, T. Deliagina, O. Ekeberg, A. El Manira, R. H. Hill, A. Lansner, G. N. Orlovsky, and P. Wallen, Trends Neurosci. **18**, 270 (1995).
[19] J. D. Wood, Jpn. J. Smooth Muscle Res. **23**, 143 (1987).
[20] M. D. Gershon and P. R. Wade, Current Opinion Gastroenterol. **9**, 246 (1993).
[21] R. N. Miftakhov and D. L. Wingate, J. Comput. Inf. **3**, 117 (1993).
[22] R. N. Miftakhov, G. R. Abdusheva, and D. L. Wingate, Biol. Cybern. **74**, 167 (1996).